C. R. Acad. Sci. Paris, Ser. I 348 (2010) 1027–1032

Contents lists available at ScienceDirect

C. R. Acad. Sci. Paris, Ser. I

www.sciencedirect.com

Numerical Analysis

A curvilinear finite-volume method to solve compressible gas dynamics in semi-Lagrangian coordinates

Volumes finis curvilignes pour la résolution des équations de la dynamique des gaz en coordonnées semi-Lagrangiennes

Stéphane Del Pino

CEA, DAM, DIF, 91297 Arpajon, France

ARTICLE INFO

Article history:
Received 27 July 2010
Accepted 17 August 2010

Presented by Olivier Pironneau

ABSTRACT

We present a new finite-volume method to solve compressible gas dynamics in semi-Lagrangian coordinates on curvilinear grids. The approach relies on a weak formulation to compute the mesh velocity using an acoustic Riemann solver approximation. We prove this method to be both conservative and entropic.

RÉSUMÉ

On présente un nouveau schéma de type volumes finis pour la résolution des équations de la dynamique des gaz en coordonnées semi-Lagrangiennes. Cette approche s'appuie sur une formulation faible permettant le calcul de la vitesse du maillage utilisant un solveur de Riemann acoustique. Cette méthode est conservative et entropique.

Version française abrégée

Il y a bien des manières de discrétiser les équations de la dynamique des gaz en coordonnées semi-Lagrangiennes (1)–(4). Généralement, on définit un maillage polygonal du domaine fluide à $t = 0$ et on utilise son schéma favori. Une hypothèse de discrétisation implicite est alors d'imposer aux arêtes de rester droites durant le calcul. Ce choix rend impossible l'écriture de schémas numériques d'ordre supérieur ou égal à 3 dans le cas général puisque l'erreur géométrique est alors du second ordre.

Cette Note, qui présente une méthode permettant de traiter des arêtes de géométrie quelconque, s'articule de la manière suivante. Tout d'abord, on décrit la méthode puis on en montre les propriétés attendues. Enfin, on illustre son fonctionnement sur deux exemples numériques.

Bien que la nature du schéma présenté soit de type volumes finis, le calcul de la vitesse continue du maillage $\mathbf{U}^\star$ utilise une méthode d'éléments finis aux arêtes. On écrit un solveur de Riemann acoustique le long des arêtes (5), et après avoir traduit cette égalité en terme de projection sur la normale $\mathbf{n}_{jl}$, on l'écrit de manière faible (7). Afin de calculer les flux : $\mathbf{U}^*$ et les $P_j^\star$, on écrit la contrainte de conservativité faiblement sur les $P_j^\star$ (8). Ce qui permet d'obtenir une formulation variationnelle sur $\mathbf{U}^\star$. Ce problème continu *global* admet une unique solution si et seulement si toutes les arêtes du maillage n'admettent aucune partie droite.

E-mail address: stephane.delpino@cea.fr.

1631-073X/$ – see front matter
doi:10.1016/j.crma.2010.08.006

On choisit ensuite de discrétiser cette formulation variationnelle en cherchant $\mathbf{U}^\star$ dans l'espace $\mathbb{P}^k$ des fonctions continues aux sommets et polynômes de Lagrange de degré k aux arêtes. On aboutit alors au système linéaire (12) qui permet de calculer la vitesse du maillage. Ce système est *inversible* à la seule condition que les supports des fonctions de base soient tous courbes. La matrice obtenue est creuse si les fonctions de base sont à support compact.

Dans le cas où des arêtes sont droites, on choisit ici de ne calculer que la vitesse normale aux degrés de liberté internes problématiques et d'y interpoler linéairement la composante tangentielle vitesse en fonction des vitesses tangentielles des sommets de l'arête. Ce choix ne change évidemment pas les propriétés du schéma, puisque seule la vitesse normale intervient dans (6).

Le schéma proposé est invariant par changement de repère Galiléen. Il est conservatif en masse, volume, impulsion et énergie totale aux conditions aux limites près. De plus, il vérifie par construction l'inégalité d'entropie. Par ailleurs, toutes ces propriétés ne reposant que sur la linéarité de l'intégrale, elles sont aussi satisfaites si on remplace les intégrales exactes par des formules de quadrature (il est seulement nécessaire d'utiliser toujours la même formule pour calculer toutes les intégrales d'une même arête).

On démontre également que le schéma proposé dégénère naturellement sur le schéma Chic [6] à l'ordre 1.

Finalement, pour illustrer le fonctionnement de la méthode, on présente deux expériences numériques : un tube à choc de Sod convergeant et une compression isentropique de Kidder. Les résultats sont présentés en Fig. 2.

1. Introduction

We first recall the compressible Euler equations in semi-Lagrangian coordinates in their integral form. Writing $d \in \{1, 2, 3\}$, we denote by $\Omega(t) \in \mathbb{R}^d$ a connected open set which represents the domain occupied by a fluid satisfying the Euler equations at any time $t \geqslant 0$. For any $\omega(t) \subset \Omega(t)$, which moves at the fluid velocity $\mathbf{u}$, one has

$$\frac{\mathrm{d}}{\mathrm{d}t}\int_{\omega(t)} 1 = \int_{\omega(t)} \nabla\cdot\mathbf{u}, \qquad \text{volume conservation} \tag{1}$$

$$\frac{\mathrm{d}}{\mathrm{d}t}\int_{\omega(t)} \rho = 0, \qquad \text{mass conservation} \tag{2}$$

$$\frac{\mathrm{d}}{\mathrm{d}t}\int_{\omega(t)} \rho\mathbf{u} = -\int_{\omega(t)} \nabla p, \qquad \text{momentum conservation} \tag{3}$$

$$\frac{\mathrm{d}}{\mathrm{d}t}\int_{\omega(t)} \rho E = -\int_{\omega(t)} \nabla\cdot p\mathbf{u}, \qquad \text{total energy conservation} \tag{4}$$

where ρ is the density, E the total energy density and $p = p(\rho, e)$ is the pressure. The internal energy density is $e = E - \frac{1}{2}\mathbf{u}\cdot\mathbf{u}$. $c = (\frac{\gamma p}{\rho})^{\frac{1}{2}}$ designates the sound speed, while γ is the adiabatic constant of the gas.

There are several ways to discretize (1)–(4). One usually defines a polygonal mesh that approximates $\Omega(0)$'s geometry and runs his favorite scheme on it. However one common implicit assumption of these methods is that initial polygonal cells remain polygonal all along the calculus. In other words, edges are kept straight. This is a choice of discretization that makes it impossible to build a scheme of order higher than two in the general case – see [2,3]. Another drawback of considering only straight edges is that practically, geometrical error of discretization can be dominant with regard to other discretization parameters (considering Kidder's test case in a converging shell for instance, convergence can be higher than one with a first-order scheme since geometrical approximation is of second order and geometrical error is dominating).

For these reasons, this Note presents a new finite-volume discretization of (1)–(4) with arbitrary cell shapes (parametrized). Others approaches to curvilinear Lagrangian schemes have been recently proposed in [3,5], but the first does not satisfy the Geometrical Conservation Law (1) and the second concerns staggered schemes for which orders higher than 3 seem difficult to reach for geometry.

This Note is planned as follows. First, we describe the method. Then, we show its expected properties. Finally, we present two numerical experiments in dimension 2: Sod's shock tube and Kidder's isentropic compression.

2. Derivation of the scheme

While the method extends naturally to 3D, we restrict here to the 2D case to simplify notations.

Following [4,6,1], the scheme relies on the use of an acoustic Riemann solver and respects the GCL (1) for the continuous in time semi-discretization.

For the sake of clarity, before presenting the approximation spaces used to define it, we precise the nature of mesh velocity approximation: while the scheme remains a finite-volume-like method, edge velocities are computed in a finite-element-like fashion on edges. Also, satisfying the GCL (1) imposes naturally the resolution of a *global* problem: a weighted L^2-projection. Obviously, choosing compactly supported basis functions leads to a sparse matrix.

2.1. Fluxes approximation

We denote by j the generic cell of a curvilinear and conforming mesh of $\Omega(t)$ and by l the generic edge. As usually in the finite-volume framework, we assume that for each cell j of the mesh one knows the two reconstructed variables: $\mathbf{U}_j(\mathbf{x})$ and $P_j(\mathbf{x})$ (respectively the reconstructed velocities and pressures). Denoting by $\mathcal{L}_j$ the set of edges l belonging to cell j, we impose the acoustic Riemann invariant relation $\mathrm{d}p + \rho c\,\mathrm{d}\mathbf{u}\cdot\mathbf{n} = 0$, which reads along any edge. Introducing $\mathbf{U}^\star$ the edges velocity and $P_j^\star$ the edge pressure imposed by cell j, we write

$$\forall j,\ \forall l \in \mathcal{L}_j,\ \forall \mathbf{x} \in l, \quad P_j^\star(\mathbf{x}) - P_j(\mathbf{x}) + (\rho c)_j\big(\mathbf{U}^\star(\mathbf{x}) - \mathbf{U}_j(\mathbf{x})\big)\cdot\mathbf{n}_{jl}(\mathbf{x}) = 0, \tag{5}$$

where $\mathbf{n}_{jl}$ is the normal to edge l outgoing from cell j. Notice that $\mathbf{n}_{jl}$ is not constant along l.

The semi-discrete scheme will then read the same as [4,6,1] except that cell-centered conservative quantities will be updated by

$$\forall j, \quad \frac{\mathrm{d}}{\mathrm{d}t}\int_j 1 = \sum_{l\in\mathcal{L}_j}\int_l \mathbf{U}^\star\cdot\mathbf{n}_{jl}, \qquad \frac{\mathrm{d}}{\mathrm{d}t}\int_j \rho\mathbf{u} = -\sum_{l\in\mathcal{L}_j}\int_l P_j^\star\mathbf{n}_{jl}, \qquad \frac{\mathrm{d}}{\mathrm{d}t}\int_j \rho E = -\sum_{l\in\mathcal{L}_j}\int_l P_j^\star\mathbf{U}^\star\cdot\mathbf{n}_{jl}. \tag{6}$$

We introduce the one-dimensional edges space $\mathcal{E} := \{\mathbf{x}/\exists l \text{ s.t. } \mathbf{x}\in l\}$. In order to preserve the mesh topology, we look for $\mathbf{U}^\star \in (C^0(\mathcal{E}))^d$. Also, according to (5), knowing $\mathbf{U}^\star$ also determines each $P_j^\star$.

2.1.1. Weak form

To derive the weak form of (5), we assume that $\mathbf{U}_j|_{\mathcal{E}} \in (L^2(\mathcal{E}))^d$, $P_j|_{\mathcal{E}} \in L^2(\mathcal{E})$, and $P_j^\star \in L^2(\mathcal{E})$. Introducing $\mathcal{V} := L^2(\mathcal{E}) \cap C^0(\mathcal{E})$, we assume $\mathbf{U}^\star \in \mathcal{V}^d$. Also we have $(\rho c)_j \in \mathbb{R}^{+,\star}$ and $\mathbf{n}_{jl} \in (L^\infty(\mathcal{E}))^d$.

So, since $\forall \mathbf{x}\in l$, $\mathbf{n}_{jl}(\mathbf{x}) \neq \mathbf{0}$, and after simple algebraic manipulations, we get

$$\forall j,\ \forall l \in \mathcal{L}_j,\ \forall \mathbf{x}\in l, \quad P_j^\star(\mathbf{x})\mathbf{n}_{jl}(\mathbf{x}) + (\rho c)_j\mathbf{n}_{jl}\otimes\mathbf{n}_{jl}(\mathbf{x})\mathbf{U}^\star(\mathbf{x}) = P_j(\mathbf{x})\mathbf{n}_{jl}(\mathbf{x}) + (\rho c)_j\mathbf{n}_{jl}\otimes\mathbf{n}_{jl}(\mathbf{x})\mathbf{U}_j(\mathbf{x}).$$

Thus, we obtain the following equivalent weak form:

$$\forall j,\ \forall l \in \mathcal{L}_j,\ \forall \phi \in \mathcal{V}, \quad \int_l P_j^\star\mathbf{n}_{jl}\phi + \int_l (\rho c)_j\mathbf{n}_{jl}\otimes\mathbf{n}_{jl}\mathbf{U}^\star\phi = \int_l P_j\mathbf{n}_{jl}\phi + \int_l (\rho c)_j\mathbf{n}_{jl}\otimes\mathbf{n}_{jl}\mathbf{U}_j\phi. \tag{7}$$

Remembering that $\mathcal{V}$ is a space of continuous functions, we impose the following conservativity constraint:

$$\forall \phi \in \mathcal{V}, \quad \sum_j\sum_{l\in\mathcal{L}_j}\int_l P_j^\star\mathbf{n}_{jl}\phi = \mathbf{0}. \tag{8}$$

Summing (7) over all edges l of all cells j leads to the variational problem on $\mathbf{U}^\star$:

$$\forall \phi \in \mathcal{V}, \quad \sum_j\sum_{l\in\mathcal{L}_j}\int_l (\rho c)_j\mathbf{n}_{jl}\otimes\mathbf{n}_{jl}\mathbf{U}^\star\phi = \sum_j\sum_{l\in\mathcal{L}_j}\int_l P_j\mathbf{n}_{jl}\phi + \sum_j\sum_{l\in\mathcal{L}_j}\int_l (\rho c)_j\mathbf{n}_{jl}\otimes\mathbf{n}_{jl}\mathbf{U}_j\phi. \tag{9}$$

Remark 1. Note that the problem: find $\mathbf{U}^\star \in \mathcal{V}^d$ s.t. (9) has a unique solution if and only if edges are never flat (support of any continuous test function $\phi \in \mathcal{V}$ must never be a straight line). On any straight portion of l the tangential component of $\mathbf{U}^\star$ is not uniquely defined.

In the following, we discretize (9) by choosing $\mathcal{V}_h \subset \mathcal{V}$ such that $\dim\mathcal{V}_h < +\infty$.

2.1.2. A $\mathbb{P}^k$ approximation of $\mathcal{V}$

We propose to discretize each component of $\mathbf{U}^\star$ using an isoparametric Lagrange finite-element approximation $\mathbb{P}^k$ on edges, k being the degree of the polynomial. Thus, we introduce $\mathcal{F}$ the set of degrees of freedom α on the edges of the mesh. The $\mathbb{P}^k$ approximation imposes that naturally the velocity $\mathbf{U}^\star \in \mathcal{V}^d$. This is traduced by the fact that each vertex of the mesh carries a degree of freedom and that some degrees of freedom are located into the interior of edges. More precisely, denoting by $\mathbf{x}_\alpha$ the position of degree of freedom α, we introduce the space of discretization $\mathcal{V}_h = \mathrm{Span}(w^\alpha)$, where

$$w^\alpha \in C^0(\mathcal{E}), \text{ and } \forall \alpha,\beta\in\mathcal{F}, \quad w^\alpha(\mathbf{x}_\beta) = \delta_{\alpha\beta}, \quad \text{and} \quad \forall \mathbf{x}\in\mathcal{E}, \quad \sum_{\alpha\in\mathcal{F}} w_\alpha(\mathbf{x}) = 1. \tag{10}$$

Moreover, the support of w^α reduces to the set of edges containing $\mathbf{x}_\alpha$. These are classically satisfied in $\mathbb{P}^k$ approximation, where w^α is obtained by a conformal transformation of the polynomial $\hat{w}^\alpha$ of $[0,1]$: $w^\alpha = \hat{w}^\alpha \circ \mathbf{T}^{l^{-1}}$. $\mathbf{T}^l$ denotes the conformal transformation $l = \mathbf{T}^l([0,1])$ and α represents both the global degree of freedom and its associate local one in $[0,1]$ to simplify notations. Fig. 1 presents examples of w^α shape functions in the case of the isoparametric-$\mathbb{P}^2$ approximation.

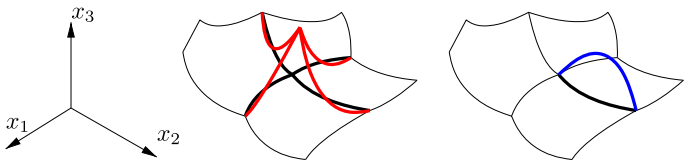

Fig. 1. Basis functions: two typical $\mathbb{P}^2$ isoparametric basis functions are represented on a curvilinear grid. A vertex located basis function in red, and an internal to the edge in blue. Their supports are depicted in heavy black.

Thus, in the approximation space, since $\mathbf{U}^\star = \sum_{\beta\in\mathcal{F}} w^\beta \mathbf{u}_\beta$, with $\mathbf{u}_\beta \in \mathbb{R}^d$, one has

$$\forall \alpha \in \mathcal{F}, \quad \sum_j \sum_{l\in\mathcal{L}_j} \int_l P_j^\star \mathbf{n}_{jl} w^\alpha = \mathbf{0}, \quad \text{and} \tag{11}$$

$$\left(\sum_j \sum_{l\in\mathcal{L}_j} \int_l (\rho c)_j \mathbf{n}_{jl} \otimes \mathbf{n}_{jl} w^\alpha w^\beta\right)\mathbf{u}_\beta = \sum_j \sum_{l\in\mathcal{L}_j} \int_l P_j \mathbf{n}_{jl} w^\alpha + \sum_j \sum_{l\in\mathcal{L}_j} \int_l (\rho c)_j \mathbf{n}_{jl} \otimes \mathbf{n}_{jl} \mathbf{U}_j w^\alpha. \tag{12}$$

One notices that to compute $\mathbf{U}^\star$, the resolution of a *global* linear system is required. However this linear system is sparse because w^α functions have compact support. Their support restricts to one edge or edges sharing a vertex – see Fig. 1. Moreover, this linear system discretizes a weighted-$L^2(\mathcal{E})$ projection operator which is known to have good condition number.

Remark 2. Notice that $(\rho c)_j \mathbf{n}_{jl} \otimes \mathbf{n}_{jl}(\mathbf{x})$ are rank 1 matrices which are symmetric and positive definite on their image subspace. So, in 2D, for any non-straight edge l, $\int_l (\rho c)_j \mathbf{n}_{jl} \otimes \mathbf{n}_{jl}(\mathbf{x})$ is a symmetric and positive definite matrix of $\mathbb{R}^{2\times 2}$. Thus, if all edges of the mesh are non-straight, the global matrix is symmetric and positive definite. So, in that case $\mathbf{U}^\star$ can be computed.

Finally we precise the mesh motion in this case: $\mathbf{x}_\alpha$ are displaced at the velocity $\mathbf{u}_\alpha$.

2.1.3. Straight edges treatment

As shown previously, finding $\mathbf{U}^\star$ satisfying (11)–(12) is not a well-posed problem if and only if an edge of the mesh is straight. A way to overcome this problem consists in solving only the normal to straight edges component of $\mathbf{U}^\star$ and to interpolate the tangential velocities of extremities. This is not yet satisfactory, but this choice does not change the scheme since the tangential component is not involved in (6).

3. Scheme properties

3.1. Galilean invariance

The scheme is Galilean invariant. Introducing $\mathbf{U}_\mathcal{G} \in \mathbb{R}^d$ a constant velocity field, one denotes that replacing the cell-data velocity $\mathbf{U}_j$ by $\mathbf{U}_\mathcal{G} + \mathbf{U}_j$ leads to the solution $\mathbf{U}^\star + \mathbf{U}_\mathcal{G}$ thanks to the linearity of operators in (9) or (12).

3.2. Conservativity

Up to the boundary conditions, the scheme is conservative in mass, volume, momentum and total energy. Mass conservation is obvious. Introducing $\mathcal{J}_l$, the set of cells j having l as an edge, one has

$$\sum_j \sum_{l\in\mathcal{L}_j} \int_l \mathbf{U}^\star \cdot \mathbf{n}_{jl} = \sum_l \sum_{j\in\mathcal{J}_l} \int_l \mathbf{U}^\star \cdot \mathbf{n}_{jl} = \sum_l \int_l \left(\mathbf{U}^\star \cdot \sum_{j\in\mathcal{J}_l} \mathbf{n}_{jl}\right) = 0,$$

$$\sum_j \sum_{l\in\mathcal{L}_j} \int_l P_j^\star \mathbf{n}_{jl} = \sum_j \sum_{l\in\mathcal{L}_j} \int_l \left(P_j^\star \mathbf{n}_{jl} \sum_{\alpha\in\mathcal{F}} w^\alpha\right) = \sum_{\alpha\in\mathcal{F}} \left(\sum_j \sum_{l\in\mathcal{L}_j} \int_l P_j^\star \mathbf{n}_{jl} w^\alpha\right) = \mathbf{0},$$

$$\sum_j \sum_{l\in\mathcal{L}_j} \int_l P_j^\star \mathbf{U}^\star \cdot \mathbf{n}_{jl} = \sum_l \sum_{j\in\mathcal{J}_l} \int_l P_j^\star \sum_{\alpha\in\mathcal{F}} w^\alpha \mathbf{u}_\alpha \cdot \mathbf{n}_{jl} = \sum_{\alpha\in\mathcal{F}} \left(\sum_j \sum_{l\in\mathcal{L}_j} \int_l P_j^\star \mathbf{n}_{jl} w^\alpha\right) \cdot \mathbf{u}_\alpha = 0.$$

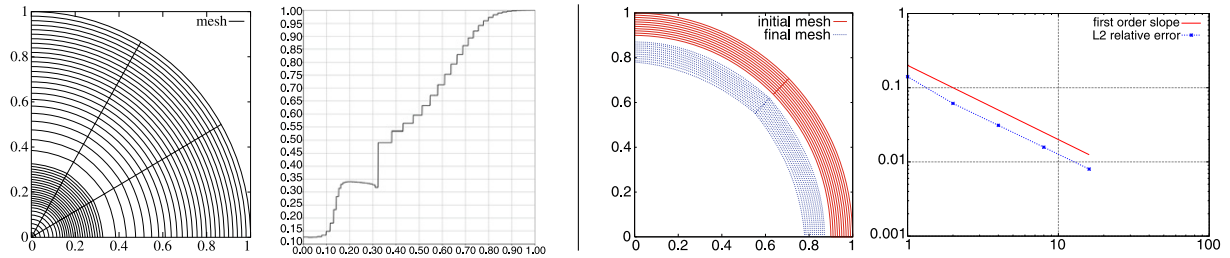

Fig. 2. Left: Sod's shock tube mesh and density profile at final time $t = 0.2$. Right: Kidder's isentropic compression. Initial and final 2×10 meshes. First-order (red) and L^2 relative error (blue), w.r.t. refinement, are plotted in log scale.

3.3. Entropy production

Also, the semi-discrete in time scheme is entropic for constant cell-centered data $\mathbf{U}_j$ and P_j. Recalling that $\int_{\omega(t)} \rho \partial_t \psi = \frac{\mathrm{d}}{\mathrm{d}t} \int_{\omega(t)} \rho\psi$ and reinterpreting $V_j \rho_j T_j \partial_t S_j = V_j \rho_j \partial_t e_j + V_j \rho_j p_j \partial_t (\frac{1}{\rho_j})$ in terms of integrals over cells, one gets using (6)

$$V_j \rho_j T_j \partial_t S_j = -\int_{\partial j(t)} \mathbf{U}^\star P_j^\star \cdot \mathbf{n} - \int_{\partial j(t)} P_j^\star \cdot \mathbf{n} + \int_{\partial j(t)} P_j \mathbf{U}^\star \cdot \mathbf{n} + \overbrace{\int_{\partial j(t)} \mathbf{U}_j P_j \cdot \mathbf{n}}^{=0}$$
$$= \int_{\partial j(t)} \big(\mathbf{U}_j - \mathbf{U}_j^\star\big) \cdot \mathbf{n}\big(P_j^\star - P_j\big) \geqslant 0 \quad \big(\text{inequality comes from (5)}\big).$$

Above, we presented the scheme using exact integration for the fluxes. However, in practice some integrals are very complex or even not possible to compute exactly (depending on the kind of curvilinear representation). Thus, integrals are replaced by quadrature formulas defined on the reference edge $[0, 1]$ using a variable change. However, presented results remain true since the only property of the integral operator that is used above is its linearity (one only needs to always use the same formula on a given edge to approximate integrals on it).

3.4. A special case

Assuming constant cell-data and straight edges, Eq. (12) simplifies to

$$\Big(\sum_j (\rho c)_j \sum_{l \in \mathcal{L}_j} \mathbf{n}_{jl} \otimes \mathbf{n}_{jl} \int_l w^\alpha w^\beta\Big)\mathbf{u}_\beta = \sum_j P_j \sum_{l \in \mathcal{L}_j} \mathbf{n}_{jl} \int_l w^\alpha + \sum_j (\rho c)_j \Big(\sum_{l \in \mathcal{L}_j} \mathbf{n}_{jl} \otimes \mathbf{n}_{jl} \int_l w^\alpha\Big)\mathbf{U}_j.$$

Then choosing $\mathcal{V} = \mathbb{P}^1$ implies that $\int_l w^\alpha = \frac{1}{2}|l|\mathbf{1}_l(\mathbf{x}_\alpha)$. If $\int_l w^\alpha w^\beta$ is approached by the trapezium formula, the linear system becomes bloc diagonal, and we obtain the first-order Chic scheme [6]:

$$\forall \alpha \in \mathcal{F}, \quad \Big(\sum_j (\rho c)_j \sum_{l \in \mathcal{L}_j} \frac{|l|}{2} \mathbf{1}_l(\mathbf{x}_\alpha) \mathbf{n}_{jl} \otimes \mathbf{n}_{jl}\Big)\mathbf{u}_\alpha = \sum_j P_j \sum_{l \in \mathcal{L}_j} \mathbf{n}_{jl} \frac{|l|}{2} \mathbf{1}_l(\mathbf{x}_\alpha) + \sum_j (\rho c)_j \Big(\sum_{l \in \mathcal{L}_j} \frac{|l|}{2} \mathbf{1}_l(\mathbf{x}_\alpha) \mathbf{n}_{jl} \otimes \mathbf{n}_{jl}\Big)\mathbf{U}_j.$$

4. Two numerical tests

Fig. 2 presents two numerical tests: a cylindrical converging Sod shock tube and a Kidder isentropic compression. For Sod's test the computational domain is a quarter of the unit disk. Initial data is $\rho = 0.125$, $p = 0.1$, for $\|\mathbf{x}\| \leqslant \frac{1}{2}$, $\rho = 1$, $p = 1$, for $\|\mathbf{x}\| > \frac{1}{2}$, and $\mathbf{u} = \mathbf{0}$. Final computational time is $t = 0.2$ s. For this test we take $\gamma = 1.4$. The computational grid is made of 3×50 cells. For Kidder's test, initial domain is the shell $0.9 < \|x\| < 1$. Initial data and boundary conditions are given in [2]. Final time is half the focusing time: $t \approx 0.108972473$ s. Convergence study is performed using dyadic meshes going from 1×5 to 16×80 cells. First-order of convergence is obtained. For these tests there is no reconstruction of cell-centered data so that the scheme is first-order accurate and edges are chosen parabolic.

5. Conclusion

In this Note we presented a new curvilinear finite-volume scheme to approximate compressible gas dynamics in semi-Lagrangian coordinates. The grid velocity is computed by a variational formulation obtained by an acoustic Riemann solver and a conservativity constraint. In practice, this weak formulation leads to a global linear system on all velocity's degrees

of freedom. The scheme is conservative and entropic, even with approximate integration. Under some discretization choices the Chic scheme [6] is retrieved.

Future work will consist in exploring deeper this method. Also, combining it with reconstruction approaches such as [2] should allow to write arbitrary high-order schemes in semi-Lagrangian coordinates.

Acknowledgements

The author is grateful to G. Carré, P. Hoch, and E. Labourasse for the fruitful discussions we had on this topic and their comments about this work.

References

[1] G. Carré, S. Del Pino, B. Després, E. Labourasse, A cell-centered Lagrangian hydrodynamics scheme in arbitrary dimension, J. Comput. Phys. 228 (14) (2009) 5160–5183.
[2] G. Carré, S. Del Pino, K. Pichon Gostaf, E. Labourasse, A.V. Shapeev, Polynomial least-square reconstruction for semi-Lagrangian cell-centered hydrodynamic schemes, ESAIM: Proc. 28 (2009) 100–116.
[3] J. Cheng, C.-W. Shu, A third order conservative Lagrangian type scheme on curvilinear meshes for the compressible Euler equations, Commun. Comput. Phys. 4 (5) (2008) 1008–1024.
[4] B. Després, C. Mazeran, Lagrangian gas dynamics in two dimensions and Lagrangian systems, Arch. Ration. Mech. Anal. 178 (2005) 327–372.
[5] V. Dobrev, T. Ellis, T. Kolev, R. Rieben, Energy conserving finite element discretizations of Lagrangian hydrodynamics. Part 1: Theoretical framework, Downloadable presentation of Multimat'09 conference.
[6] P.-H. Maire, R. Abgrall, J. Breil, J. Ovadia, A cell-centered Lagrangian scheme for two-dimensional compressible flow problems, SIAM J. Sci. Comput. 29 (4) (2007) 1781–1824.